33RD CONGRESS
OF THE INTERNATIONAL COUNCIL
OF THE AERONAUTICAL SCIENCES
STOCKHOLM, SWEDEN, 4-9 SEPTEMBER, 2022

ICAS 2022 SWEDEN

MDAO OF A TRANSONIC TRUSS-BRACED WING VISION VEHICLE

David S. Lazzara[1] & Neal A. Harrison[2]

[1]Boeing Research & Technology
[2]Boeing Research & Technology

Abstract

A multidisciplinary design, analysis and optimization framework is presented for design exploration of transonic truss-braced wing configurations. Its analysis and design capabilities include multifidelity geometry management, aerodynamic shape optimization, low-speed and buffet performance predictions, stability and control constraints, mass properties, structural considerations, and mission performance. Methods were represented by direct implementation in the framework or via radial basis function surrogate modeling to enable the design of 3D geometry using higher fidelity data. A design exploration case study of transonic truss-braced wing planforms is presented that successfully demonstrates the framework capabilities.

Keywords: transonic truss-braced wing, MDAO

1 Introduction

Since the advent of the commercial aircraft market, airlines have sought to improve the capabilities of the aircraft in their fleets. These advances took many forms, including improvements to aircraft speed, range, and payload. As a means to this end, designers worked to improve the aerodynamic efficiency of these aircraft. Over many decades the progressive improvement of the standard tube-and-cantilevered wing aircraft configuration has refined the design of modern transport aircraft to the point that there are progressively smaller differences between configurations as time has passed. This process has been assisted by increasingly powerful computational tools and capabilities which can squeeze out the configuration's remaining available performance improvements. As a consequence, designs are converging on a relatively narrow design space and are facing increasing challenges to achieve significant leaps in vehicle performance. At this level, the aircraft design problem is best viewed holistically, with optimum aerodynamic performance balanced with other parameters such as direct operating costs, ease of manufacturability, and production rate as primary considerations. Due to the complex interdependencies of these parameters, these studies are increasingly conducted through the use of multi-disciplinary design tools that can probe the large and complex design space beyond which designers can reconcile through simple design trades.

In recent years increasing attention and concern has been focused on sustainability and the impact of aircraft on the environment. Commercial aircraft manufacturers are working diligently to make their product offerings increasingly efficient and cost-effective. However, the commercial aircraft market is becoming increasingly competitive. Significant leaps in performance come at either considerable cost or considerable complexity, or both. Since non-standard aircraft configurations carry a high degree of uncertainty regarding their potential performance, aircraft manufacturers are not heavily incentivized to take significant risks in abandoning the standard cantilever-wing aircraft model.

To help encourage the adoption of advanced technologies, in 2008 NASA's Advanced Air Transport Technology (AATT) group initiated a study to identify and mature configurations or technologies that had a significant potential for dramatic improvements to vehicle efficiency, emissions, and noise. The program was targeted to work with industry to mature advanced technologies to the point where they could be considered for a potential future product. Through this program Boeing and NASA collaborated on a suite of technologies as a part of the Subsonic Ultra Green Aircraft Research (SUGAR)

configuration [1, 2, 3, 4, 6, 10, 11]. Beginning with a Mach 0.70 design, a family of configurations was developed to compare detailed performance analysis, noise, emissions, and technology risk. These included gas turbine, electric, and hybrid-electric propulsion concepts, as well as cantilever-wing, blended-wing, and truss-braced wing configurations. A set of technology roadmaps was developed for the most promising technologies. As subsequent phases of SUGAR development were undertaken, the program gradually increased its focus on the development of the Transonic Truss-Braced Wing (TTBW) concept. The most recent phase of SUGAR TTBW development has focused on a Mach 0.8 design, with investigations studying aspects of both high- and low-speed performance [10, 11]. For the work presented in this paper, a Mach 0.79 TTBW vehicle was used for wing and truss planform studies and optimization.

As compared to a conventional cantilevered-wing aircraft configuration, the TTBW aircraft concept promises dramatic reductions in fuel burn due to its truss-braced high-aspect-ratio wing. The increase in wing aspect ratio has a dramatic effect on reducing vehicle induced drag, while the truss assembly significantly reduces the wing root bending moment commonly associated with high-span wing designs. By providing structural relief to the wing the configuration is able to avoid a weight penalty that would otherwise be incurred. However, the supporting truss incurs its own weight and parasitic drag penalty, thereby requiring the designer to consider overall system performance as a prime objective. Design tradeoffs between the wing and truss design become evident as the aerodynamic, structural, and mass properties must be balanced for a feasible net improvement in system-level mission performance. Multidisciplinary design, analysis, and optimization (MDAO) methods are well suited to address the design of complex systems of this type, combining automated analysis capabilities of varying fidelity, high-dimensional design space sensitivities and models, multiple objective formulations, and explicit constraints.

Multidisciplinary design of a TTBW configuration has been the focus of many MDAO efforts in the literature [5]. Concept studies included the use of high-fidelity computational fluid dynamics (CFD) with RANS [13] models, finite element methods (FEM) for structural analysis with Euler aerodynamic models [12], as well as lower fidelity aerodynamics with vortex lattice models [19] or multifidelity approaches that included static, gust, and flutter analysis [20]. Other studies focused on the effect of variable-camber continuous trailing edge flaps on TTBW configurations [17, 18, 7, 8] and aeroelastic constraints in the design problem [14]. Parametric models for structural weight [16] and predictions of jig shape [9, 21] for TTBW planforms have also been studied. These contributions shed light on many specific aerodynamic and structural nuances that are unique to TTBW configurations compared to conventional aircraft. In this effort a MDAO framework was developed with similar engineering disciplines in mind. However, a unique mixture of high-fidelity aerodynamic shape optimization with low-speed stall and buffet modeling, as well as structural analysis and surrogate modeling based on high-fidelity mass properties and mission performance methods have resulted in a design exploration capability for TTBW that encompasses both conceptual and preliminary design considerations.

Various modeling requirements across multiple engineering disciplines were applied to reduce uncertainty in the MDAO process in this work. Aerodynamic coupling between the wing and truss was a critical consideration. Classical aerodynamic analysis methods, such as vortex lattice and panel methods, could model this for lift estimates yet did not provide sufficient fidelity when corrected for compressibility effects, such as using a Karman-Tsien model, to inform 3D surface design decisions. The issue of transonic wave drag, as well as shock-boundary layer interaction, near the wing-truss intersection required sufficient geometric fidelity for a 3D computational fluid dynamics (CFD) analysis to inform aerodynamic shape optimization. This important detail was a driving requirement in the MDAO framework created here despite its departure from classic MDAO approaches seeking to avoid the computational expense it creates. An evaluation of structural integrity was also a driving requirement given the unique feature of a wing-truss assembly. This requirement introduced the need for models of mass properties, external loads, internal loads, and mission performance that were cycled in a converging loop for consistent results. The thin high-aspect ratio wings typical of TTBW configurations also warranted the need for low-speed and buffet model assessments that could potentially constrain high-speed aerodynamic performance. Lastly, geometry management became a key underlying feature of the MDAO framework in order to provide each analysis method consistent

representations of the TTBW model with the geometry fidelity they required.
This paper presents a MDAO framework for a TTBW vision system and is organized as follows. Section 2 describes the geometry management and TTBW model used. Section 3 presents the various engineering models used in the framework with subsections describing aerodynamic analysis and shape optimization, external and internal loads, mass properties, low-speed and buffet assessments, stability and control, and mission performance. Section 4 reviews a planform optimization case study to demonstrate the functionality of the MDAO framework, followed by a summary in Section 5.

2 Geometry Management

Automated geometry management in the MDAO framework ensured that all analysis methods utilized consistent representations of a TTBW model instance anywhere in the design space. As depicted in Figure 1, this was done by parameterizing a single geometry representation of the seed TTBW model and using it as the common source for additional representations of varying geometric fidelity. Each time the parameterization was updated for a new design instance, the seed model was regenerated and new models of different geometric fidelity were created that inherited the geometric properties of the parent model. In this section the fuselage, wing, truss, and empennage models are described with their corresponding parameterizations. A nacelle model was undergoing development during this effort and reserved for usage in a later design study. The multifidelity geometry necessary for aerodynamic shape optimization, low-speed and buffet analysis, mission performance and mass properties assessments, and structural analysis with a finite element method (FEM) are also explained.

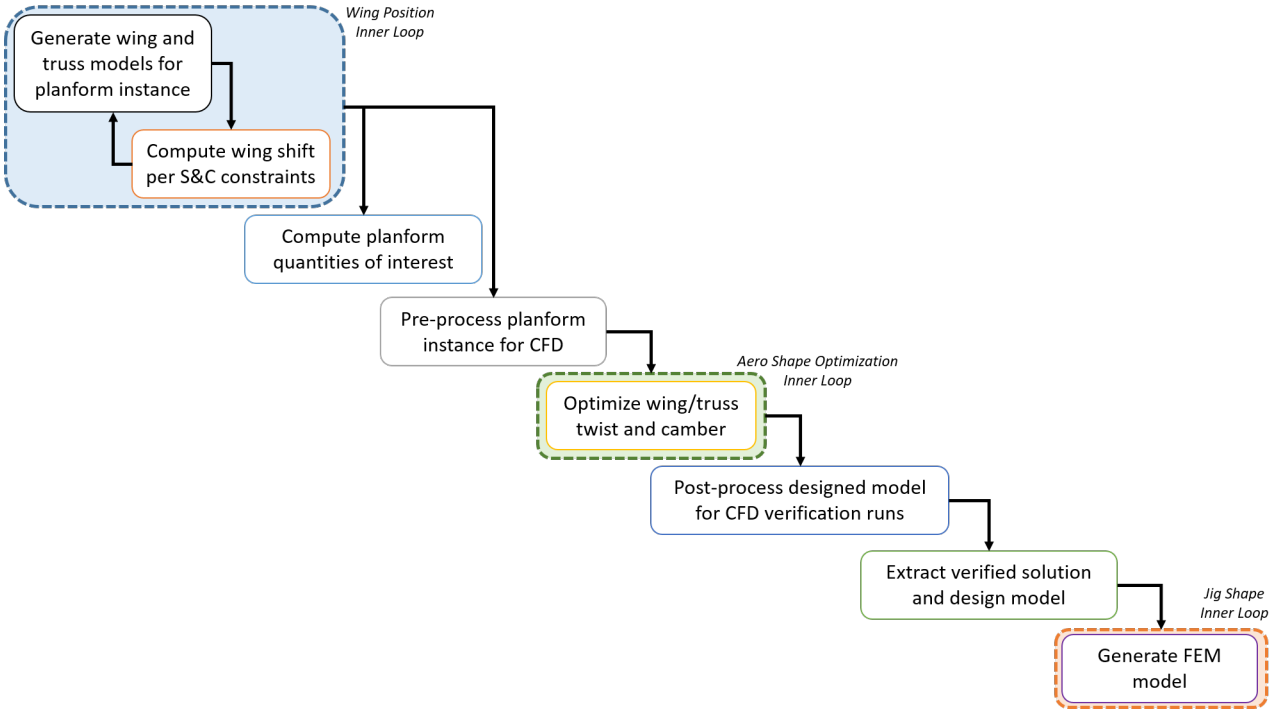

Figure 1 – Geometry representations of varying fidelity were sourced from a single seed model for consistent analysis of each planform instance.

2.1 Fuselage Model

A single fuselage model was used in this study that contained the over-sized crown fairing shown in Figure 2a such that the entire wing root would have a closed intersection curve regardless of the wing position between a predetermined range of longitudinal coordinates $[x_{min}, x_{max}]$. A smaller fairing would lead to non-planar intersections that violated mesh generation constraints of the wing root near those boundaries, as shown in Figures 2b and 2c. A reduction of the wing position range would prevent this, but doing so would hinder meaningful planform exploration. The over-sized fairing also enabled reuse of existing mesh generation tools that specialized in low-wing intersections with a fuselage and fairing. Subsequently all design instances in this study were penalized with equivalent

increases in parasite drag introduced by the oversized fairing model. Once the wing root was finalized at the end of planform design exploration, the over-sized fairing could be replaced with a customized smaller fairing that tuned performance with minimized drag while maintaining carry-over lift above the fuselage. The seed fuselage model was not modified during design exploration.

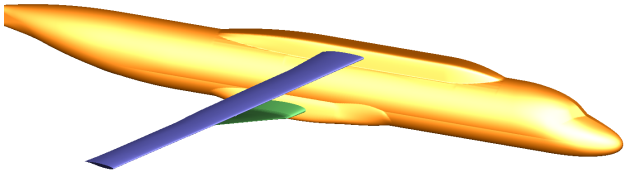

(a) Over-sized crown fairing on fuselage.

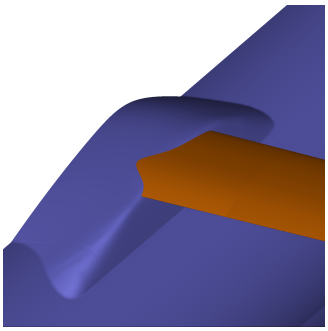

(b) Non-planar wing intersection curve on small fairing due to aft wing shift.

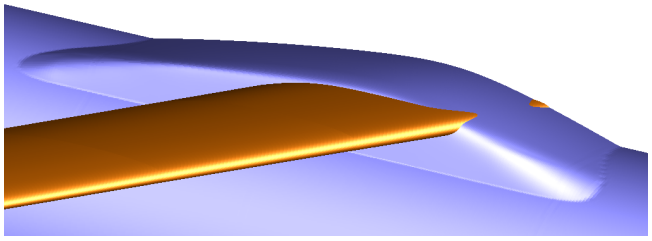

(c) Non-planar wing intersection curve on small fairing due to forward wing shift.

Figure 2 – The over-sized crown fairing enabled broader design space exploration of wing planforms without violating preset mesh constraints.

2.2 Wing and Truss Models

The wing and truss models were generated from a seed airfoil stack previously designed for Mach 0.8 with a thickness adjustment correlating with wing sweep. Seed camber and twist distributions were defined for wing airfoils in a wing reference frame and subsequently mapped to spatial locations according to a planform parameterization. Truss airfoils were initially defined with camber and twist distributions across disjointed truss reference frames in three zones, as shown in Figure 3, due to the significant variation in dihedral along its span. Each set of truss airfoils was also subsequently mapped to their correct spatial orientation via its own planform parameterization. The wing-truss assembly was parameterized with eight planform variables listed in Table 1. Variables x_1 through x_7 parameterized three adjacent trapezoidal sections along the wing span and x_8 parameterized the truss planform. With the exception of design variables x_5 and x_7, the parameterization operated as multipliers on the corresponding seed values used to generate the seed configuration. In particular, x_6 was given a large upper bound multiplier to enable a wing taper-ratio of 1 if desired.

When assembling the wing-truss-fuselage system a stability and control assessment was conducted to determine the wing longitudinal position. Each design instance was constrained to trim pitching moment about the same percentage of mean aerodynamic chord and moment reference center as the seed geometry model. The horizontal tail longitudinal position was also constrained to match that of

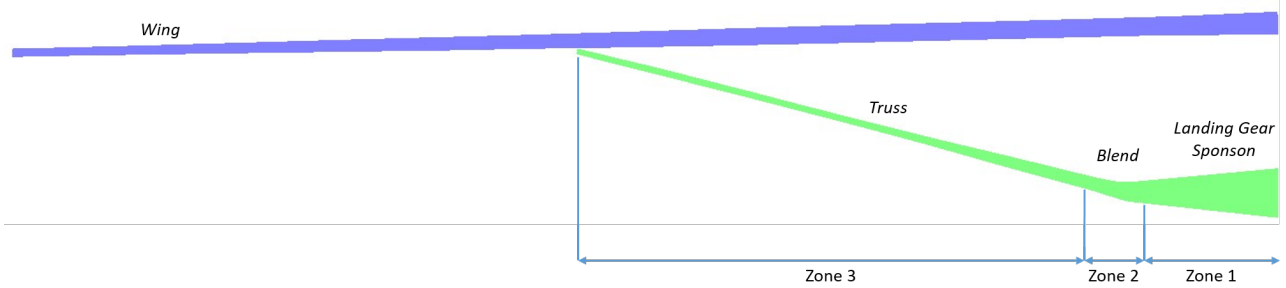

Figure 3 – Three zones along the truss span were defined as separate reference frames for airfoil camber and twist distributions.

Design Variable	Planform Variable	Lower Bound	Upper Bound
x_1	Wing Sweep	-20%	+20%
x_2	Wing Aspect Ratio	-20%	+20%
x_3	Wing Area	-20%	+20%
x_4	Root Chord	0.0	+20%
x_5	Planform Break 1 Eta	0.0	+20%
x_6	Tip Chord	-25%	+150%
x_7	Planform Break 2 Eta	0.0	+20%
x_8	Truss Attach Eta	-10%	+33%

Table 1 – Wing and truss parameterization with side bounds relative to the seed model planform.

the seed geometry model. These constraints were satisfied after converging the wing-truss-fuselage system via a fast iterative procedure that assessed pitching moment for different wing positions after regenerating the truss planform in a consistent manner each time.

The truss attachment location along the wing was constrained to have its tip leading-edge offset from the wing leading edge by coordinates $(x(y), z(y))_{\text{offset}}$ that varied with span-wise coordinate y after generating the wing geometry in each design instance. The truss tip was not intended to intersect the wing, however, in this study. This decision stemmed from prior CFD studies indicating that the flow field near the junction region was only slightly modified by the presence of an aerodynamic fairing that structurally connected the wing lower surface to the truss. Thus the wing-truss surfaces could be geometrically decoupled for easier mesh generation and flow modeling while maintaining strong aerodynamic coupling across the truss span. Once a planform was finalized a customized aerodynamic fairing could be added to connect the wing and truss.

Variable x_8 was used in a series of geometry constraints that scaled the truss airfoil stack along its span and set the truss sweep. Additional chord distribution variables were deactivated in this study to limit the truss design space. The landing gear sponson was fixed in space with only small camber and twist modifications allowed to its airfoils due to internal keep-out zones.

2.3 Empennage Model

A basic horizontal stabilizer model with trapezoidal planform was also a reused component in each design instance. No parameterization of the empennage geometry was defined except for its incidence angle, which was used during the aerodynamic shape optimization to maintain trim at the design flight condition for each instance of the wing-truss assembly.

2.4 Aerodynamic Shape Optimization Geometry Representation

The output from the wing and truss geometry routines, as well as the fuselage model, were quadrilateral mesh representations used for surface interpolation in a CFD geometry pre-processor. These surfaces became the reference for a different quadrilateral mesh network that was tuned for CFD analysis using the Boeing full potential solver Tranair [15]. Cap grids, wake networks, intersections

between the wing and truss to the fuselage, and volume meshing were all automatically generated by the pre-processor.
In addition to using the resultant discretized domain for CFD analysis, it was also the starting point for the Tranair design framework when conducting aerodynamic shape optimization of camber and twist on the wing and truss. These airfoil shape modifications were modeled with smooth basis functions across the wing and truss mesh in both chord-wise and span-wise directions, as shown in Figure 4. The designed surface meshes were an output to the optimization process, however internally intermediate modifications to the baseline model were represented as transpiration boundary conditions that modified the integral boundary layer and potential flow of each solution.

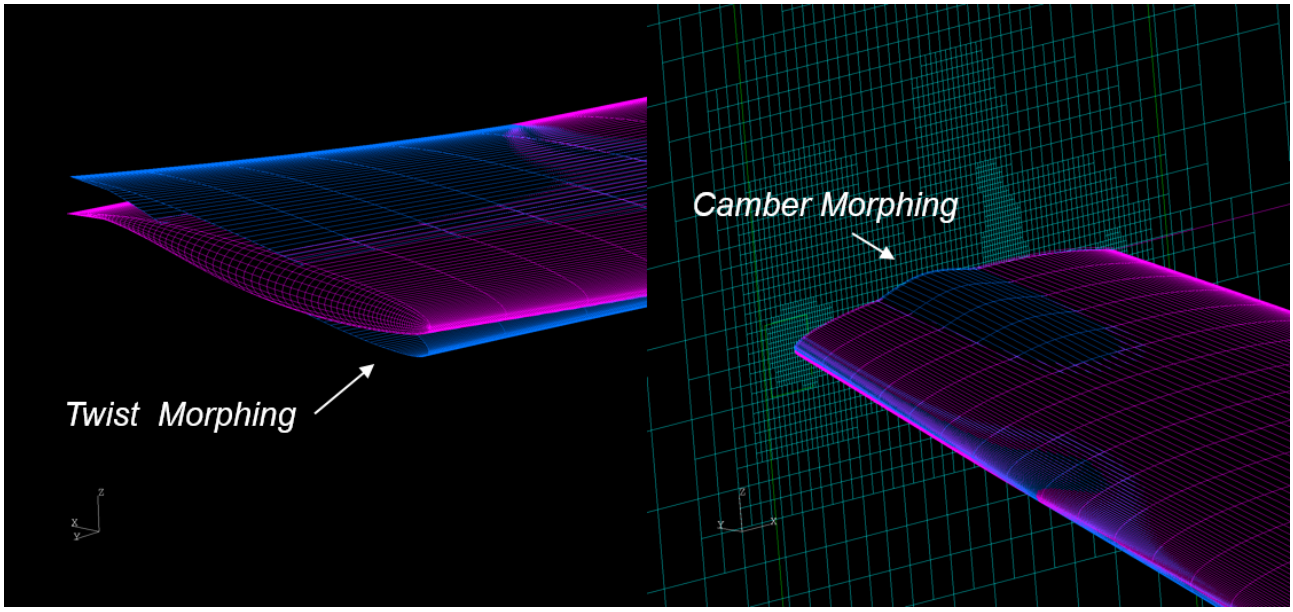

Figure 4 – Airfoil camber and twist distributions were modified with smooth basis functions across a surface mesh by the Tranair design framework.

The aerodynamic performance of the designed model was verified in a subsequent Tranair flow solution due to the potential for transpiration errors to accumulate across the optimization search path. Designed wing and truss meshes were post-processed by the CFD geometry pre-processor tools to generate a new discretized domain prior to conducting that analysis. These also served as the new reference geometry when preparing model representations for subsequent multidisciplinary analysis, thereby completing the performance description of a planform design instance.

2.5 Low-speed & Buffet Geometry Representation

Post-optimization Tranair flow solutions were processed to extract the flow state variables along the designed wing and truss surface meshes. The mesh and solution data from a low-speed solution were passed to a low-speed aerodynamics model, whereas solution and mesh data from a cruise scenario with higher lift-coefficient were passed to a separate buffet model. Each model analyzed their respective flow states on the design meshes.

2.6 Finite Element Geometry Representation

The designed meshes were also post-processed to extract airfoil camber, thickness, and twist along the wing and truss span. Combined with the leading and trailing edge definitions from the planform, this geometric data was passed to a pre-processor to automatically update a finite element beam model for each aero-optimized planform instance. Mass properties spatial distributions were also updated accordingly to be consistent with each instance of the beam model. Within the Nastran solution 144 process the geometry data informed a doublet-lattice model to compute a linear aerodynamic solution. Thereafter aerodynamic loads were added to the mass properties loads on the same beam-model to compute shear, moment, torsion, and deflection distributions of the structural model.

2.7 Mission Performance Geometry Representation

Surrogate models representing various mission performance metrics contained an input space that included the combined wing and truss planform area as well as wing aspect ratio. This information was computed for each planform instance using the extracted leading and trailing edge data from the finite element geometry representation.

3 Analysis Methods

Multiple engineering analysis methods were represented in the MDAO framework. As shown in Figure 5, a suite of aerodynamic, structural, stability and control, mass properties, and mission performance quantities of interest were computed that factored into the objective function and constraint definitions for planform design exploration. Each method was selected based on recommendations from subject matter experts with experience applying or developing it. In certain instances customization, automation, and other improvements were made to suit a method for analysis of TTBW configurations. Subject matter experts consulted in the implementation of each method within the MDAO framework and verified that the automated inputs of data and computed outputs were consistent with results obtained in a manual environment.

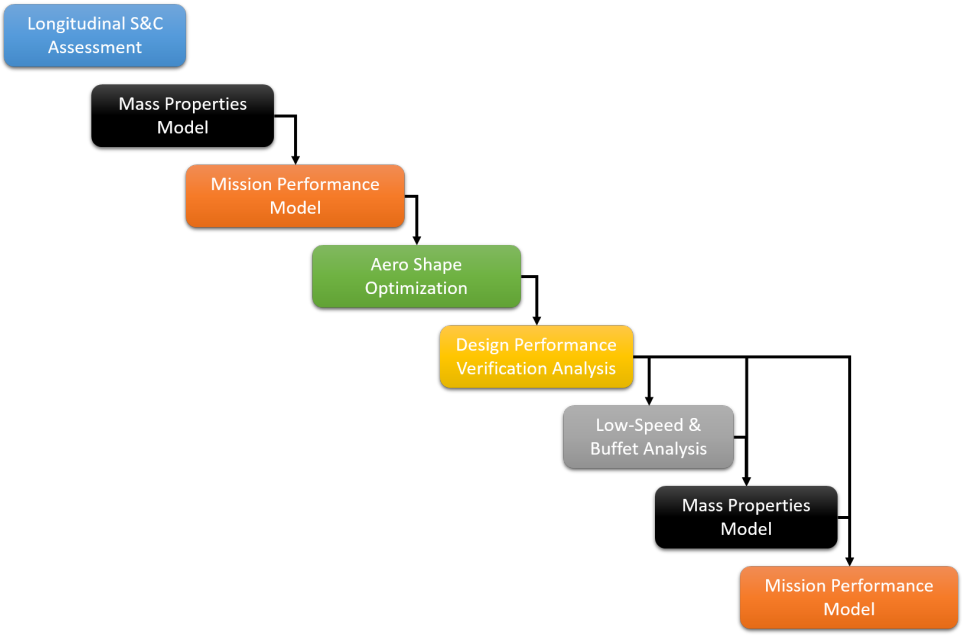

Figure 5 – A sequence of multidisciplinary analysis methods provided relevant quantities of interest for design exploration of TTBW vision vehicle planforms.

When a planform instance is defined with new parameterization values, an automated script process is launched on a high performance computing node that manages both the geometry generation sequence and the analysis method execution. The flow of geometry representations to their intended analysis method are depicted in Figure 6 with process execution commencing in the top-left of the flow chart. Both coarse and fine parallelism are implemented, along with automated disk storage management, such that the full analysis suite for a planform instance is contained within the memory and processor footprint of a single compute node on a computing cluster, thereby enabling concurrent evaluations across a cluster of numerous planform instances during design exploration.

The execution time varied across the analysis methods, as shown in Table 2, with the inner-loop aerodynamic shape optimization requiring the most. Contrary to traditional MDAO approaches that emphasize lower-fidelity analyses for fast system-level conceptual assessments, the MDAO framework in this effort was required to capture 3D compressibility effects and lift distributions directly influenced by surface shaping for any instance of a wing-truss planform. This framework was also required to output 3D surface geometry of the wing and strut for subsequent design refinements in addition to mission performance evaluations of a planform. Together these requirements created a

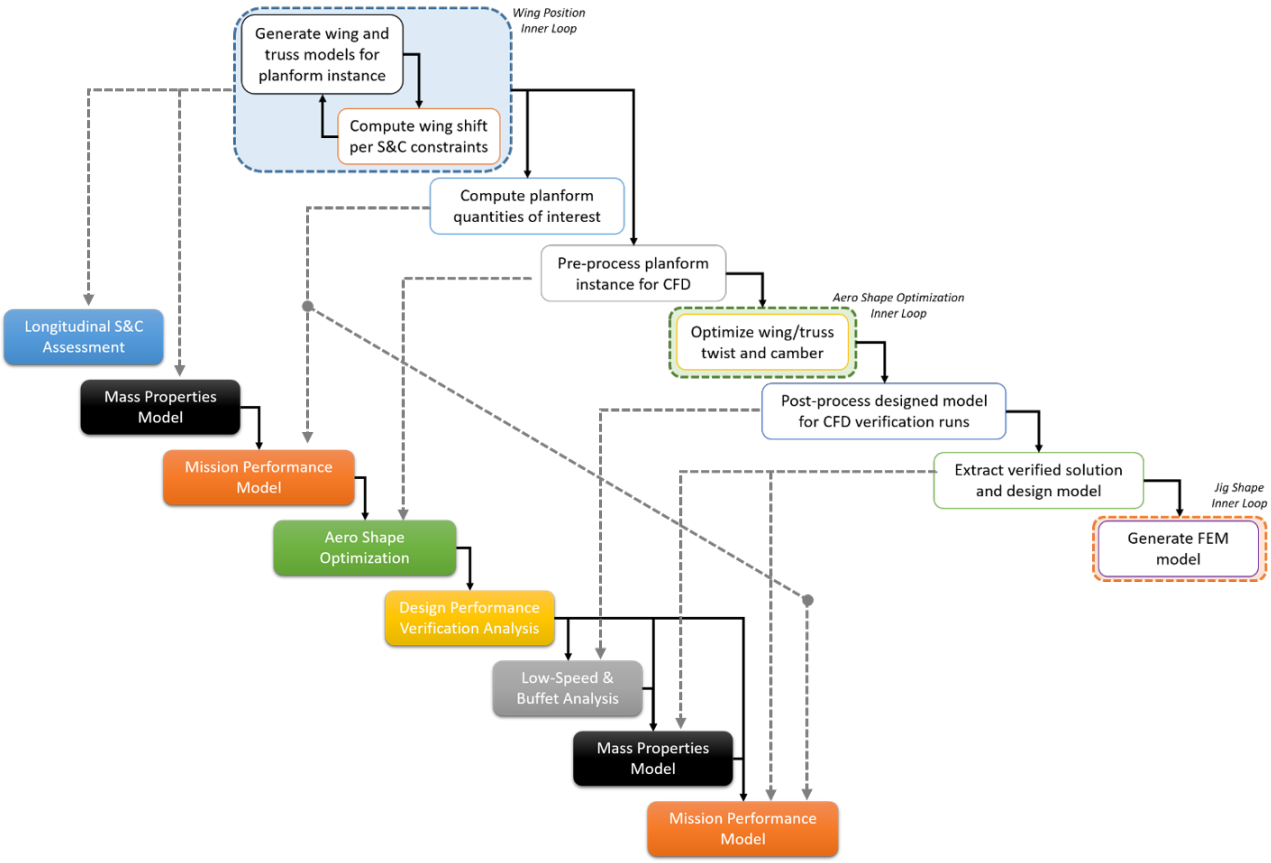

Figure 6 – An automated script process manages the creation of multifidelity geometry representations and the execution of analysis methods within the resources of a single high performance computing node.

need for comparisons of aero-optimized planforms to better capture the effects of planform variables on mission performance during design exploration. Otherwise planform comparisons risked obfuscating these sensitivities due to the impact of mistuned camber and twist distributions on aerodynamic performance.

Method	**Typical Run Time**
Geometry Generation Process	10 minutes
S&C Wing Shift Process	30 seconds
Weights Surrogate Evaluation	2 seconds
Mission Surrogate Evaluation	2 seconds
Multi-Point Aero Shape Optimization Process	3-5 days
Post-process Designed Model Geometry	10 minutes
Design Performance Verification Process	3 hours
Low-speed & Buffet Analysis	10 seconds

Table 2 – A run-time summary for each method or process in the MDAO framework, with aerodynamic shape optimization dominating the overall assessment of planform instances.

In order to determine what nominal flight conditions and lift-coefficient the aerodynamic shape optimization should utilize for a new planform instance, a mass properties estimate was obtained and a mission performance assessment was made. The optimum altitude, nominal flight conditions, and design lift-coefficient were thereby determined such that the planform aerodynamic performance was maximal when compared to other planforms. Once the shape optimization process was completed, the mass properties and mission performance methods assessed the designed model to provide its

final performance values.

3.1 Aerodynamic Shape Optimization Method

Both CFD analysis and aerodynamic shape optimization were conducted using a Boeing full potential flow solver called Tranair [15]. The solver operates on a Cartesian volume mesh that undergoes refinement based on adjoint sensitivities relative to the flow state. It also implements an integral boundary layer (IBL) method coupled with the potential flow on the chord-wise branches of quadrilateral surface networks for lifting surfaces and along fuselage surfaces, as shown in Figure 7. This provides an estimate of viscous drag with robustness to flow separation in many instances, however certain configuration regions with strong shock-induced boundary layer separation occasionally require deactivating the IBL method in that area. Added uncertainty in the absolute viscous drag estimate thus occurs in such cases, yet increment drag changes due to flow-field modifications elsewhere are potentially still valid. Wave drag, induced drag, and pressure drag are estimated from the full potential solution. A constant lift-coefficient analysis is conducted during the solution procedure by iterating on angle of attack, and a trimmed pitching-moment is also possible by iterating on the incidence of a tail surface definition. Tranair uses a Newton solver to converge a flow solution to machine precision.

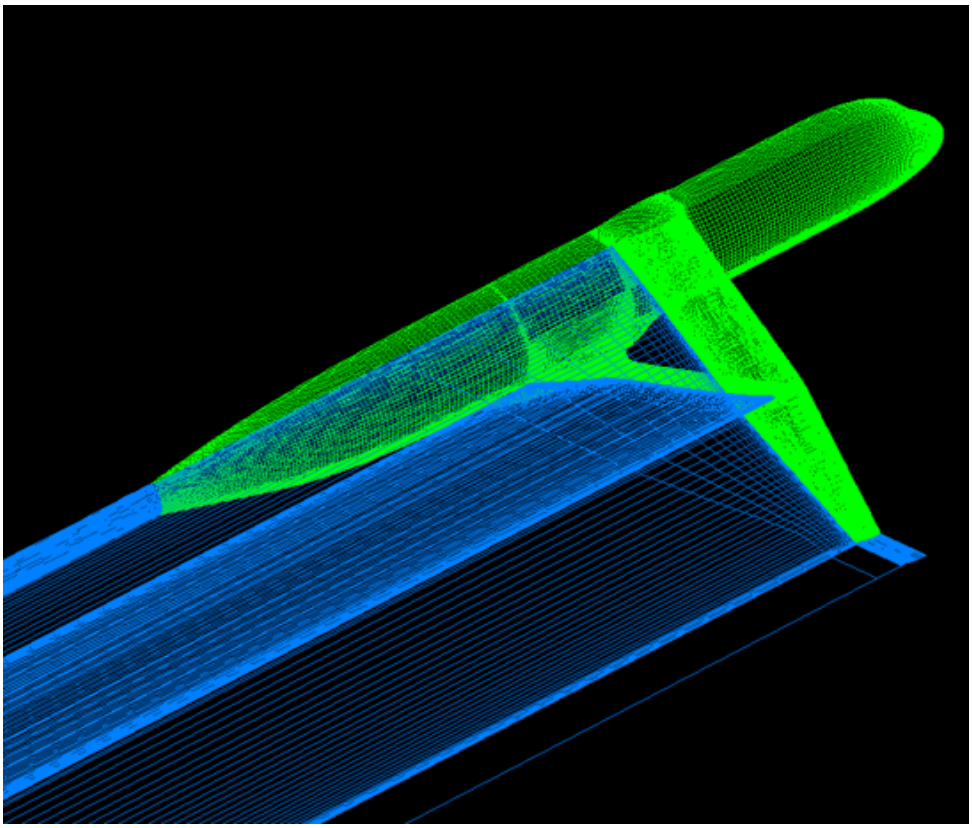

Figure 7 – An example Tranair surface mesh of a TTBW model.

A single- or multi-point analysis capability is also available within the self-contained Tranair design framework. This framework requires user-defined objective functions and constraints that utilize a variety of quantities of interest computed by the flow solver, model geometry assessments, and user-defined functions called externally. Smooth shape modifications for camber, twist, or thickness are predefined for lifting surfaces if user-defined mesh morphing is unavailable. Mesh sensitivities are automatically computed and combined via chain-rule to adjoint sensitivities in order to compute total sensitivities of quantities of interest to design variables. In multi-point design scenarios, quantities of interest calculated for different flight conditions are available to build objective functions and constraints as weighted linear combinations of outputs.

The Tranair design efforts in this study benefited from prior experience using Tranair to conduct aerodynamic shape optimization of a Mach 0.8 TTBW loft. The previous design effort sought to improve

aerodynamic performance while allowing thickness to vary on the wing and truss without violating known stiffness criteria. This included developing a low-fidelity structural model of a 2D wing box embedded in airfoils extracted from arbitrary span-wise mesh locations, as shown in Figure 8. An inner-loop gradient-based structural box optimization was added for each outer-loop aerodynamic design instance of camber, twist, and thickness distributions. As illustrated in Figure 9, it determined the optimum spar and skin thickness geometry for minimum weight at the selected span-wise stations while subject to bending and torsional stiffness constraints stemming from a previously computed high-fidelity finite-element analysis. The same setup was also utilized to determine span-wise locations of a jury strut based on different material stiffness assigned to the outboard portion of the truss structural box.

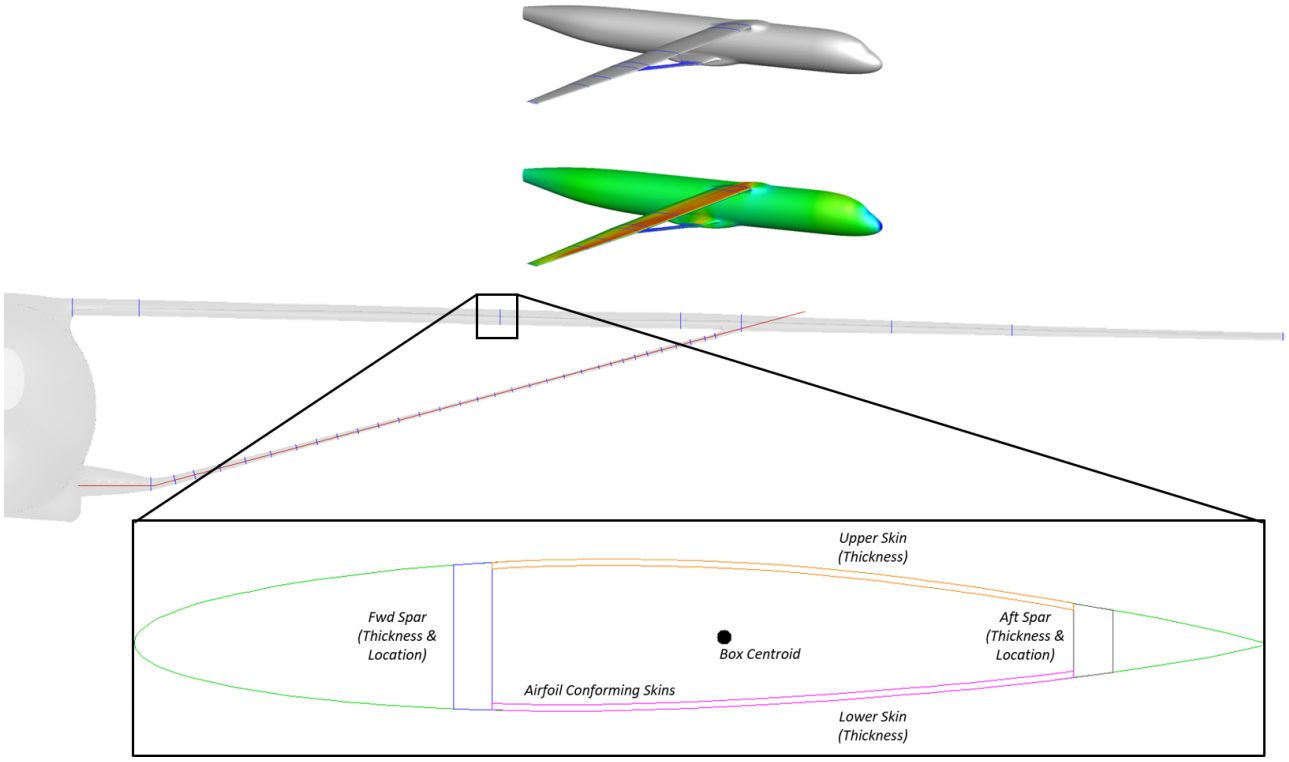

Figure 8 – Example sites of airfoil extraction from a Tranair surface mesh and subsequent embedding of a parameterized wing box for stiffness-constrained minimization of its weight across the span.

The multi-point design problem in this study was defined with a weighted objective function minimizing drag at a nominal flight condition and four off-design conditions while subject to explicit constraints on lift-coefficient, zero pitching moment, low-speed surface pressures, and surface curvature, among others. Camber and twist distributions along the wing and truss span were modified using design variables driving smooth morphing functions. Within the Tranair solution procedure the designed surfaces were modeled with transpiration boundary conditions. At the end of the optimization process the designed surface meshes were available for post-processing. Only nine design iterations were permitted for the optimizer to improve aerodynamic performance for each planform instance.

3.2 Design Performance Verification Method

Due to the accumulation of transpiration errors when modeling camber and twist modifications over multiple design iterations in the Tranair optimization, a set of verification analyses were conducted on the designed model after the optimization. The designed model was relofted and a new surface was created for Tranair analysis. The same flight conditions used in the optimization problem were repeated with the new model. A buffet condition and three other off-design conditions were also checked. The results from these cases were considered the highest-fidelity assessment of aerodynamic performance for new planforms studied within the MDAO framework.

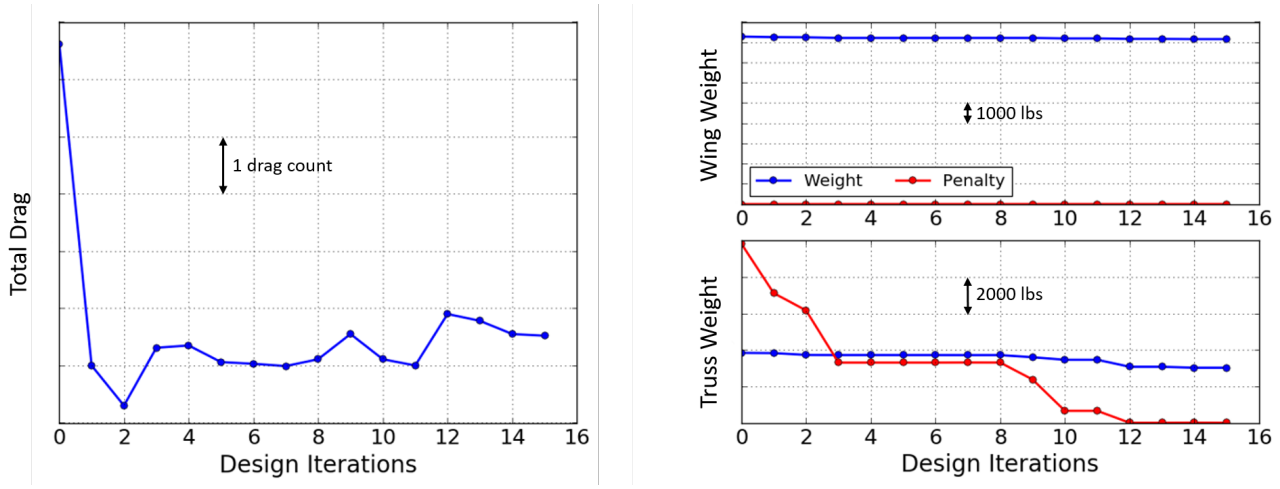

Figure 9 – Example multiobjective optimization of a TTBW model with concurrent drag minimization and stiffness-constrained minimization of structural box weight.

3.3 Low-speed & Buffet Method

The solutions from the design performance verification analyses were post-processed to generate inputs for a separate low-speed and buffet analysis method. Both methods assessed the designed wing or truss geometry in isolation as well as the flow state on their surface. The low-speed method considered the effect of leading edge curvature and minimum pressure with a model that estimates maximum lift-coefficient. The buffet method utilized an empirical model to estimate the possibility of shock-induced boundary layer separation after detecting the presence of shocks in the solution of the buffet flight condition. The results from both methods were used to flag infeasible planform candidates that would likely exhibit poor low-speed or buffet characteristics.

3.4 Mass Properties Method

A mass properties method was initially utilized that contained mass and center of gravity (CG) estimates for planform instances based on parametric weights methods, loads from a structural finite element model, and presumed structural box sizing on the wing and truss. Various assumed factors of safety, material selections, structural layout, and configuration sub-systems layout were included in these assessments. Particular assumptions were studied to determine their applicability within the design space of possible planforms investigated in this study.

The mass properties method was not integrated as an automated analysis module in the MDAO framework due to access restrictions. A solution was derived that involved building surrogate models of quantities of interest from the mass properties method as a function of planform design variables. Over 500 Latin hypercube sample planforms were generated and processed by the mass properties methods to provide estimates of operating empty weight (OEW), fuel available, and the longitudinal and vertical coordinates of center of gravity. Radial basis functions (RBF) were used to interpolate each of these outputs to create a surrogate model. Sixty-four of the sample planforms were withheld from the RBF training set and used as validation cases by directly computing the same outputs using the original mass properties method instead. Figure 10 illustrates 2D contours obtained from sampling each RBF model and showing slices with respect to wing area and wing span. The symbols depict the training and validation samples. The validation cases had acceptable model sampling errors as shown in Figure 11. The few outlier cases were found to be extreme planform candidates that may incur higher uncertainty due to assumptions in the mass properties method.

3.5 Mission Performance Method

A monolithic mission performance method was utilized to incorporate aerodynamic, mass properties, stability and control, and propulsion models to simulate flight of a TTBW model across an entire mission profile. The method was also omitted from the MDAO framework, however, due to its extensive complexity and connectivity to a different computing environment. An automated driver for the

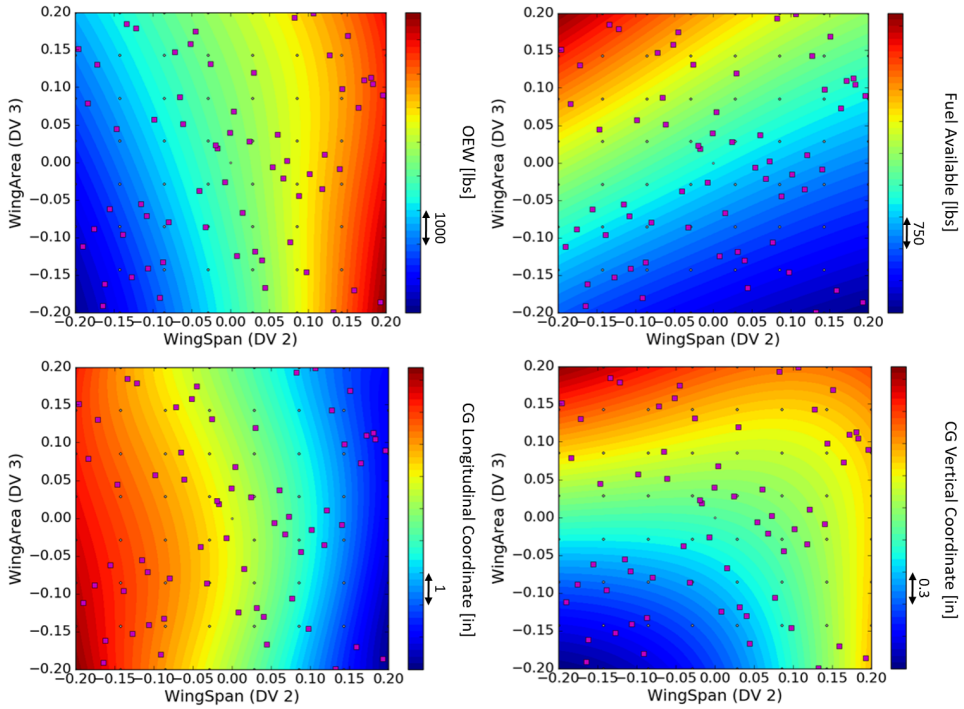

Figure 10 – RBF surrogate models, training samples (circles), and validation samples (squares) representing outputs from the mass properties method.

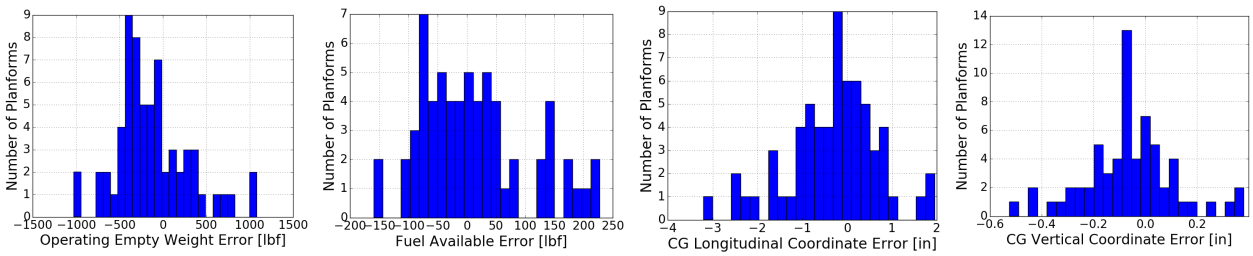

Figure 11 – Histograms of the output error between the RBF model and mass properties method predictions from the validation cases, with outliers attributed to more extreme planforms that may incur higher uncertainty in the method.

framework was developed in its native environment instead in order to update a seed TTBW model with new wing and truss planform areas and OEW estimates. Over 1000 Latin hypercube planform samples were created and processed by the mission performance method in this manner. The relevant variables in this effort were total planform area and OEW, which was obtained by processing sample planforms with the mass properties method, while the remaining configuration features of a TTBW seed model were unchanged. During this effort the internal aerodynamic database for the seed model could not be updated to reflect different planforms, thus only an update to drag estimates at specified lift-coefficient were feasible to apply at the time. An approach for updating the aerodynamic database for each planform is reserved for a future study. Furthermore, the mission performance results included a scaled horizontal stabilizer based on the provided planform area for consistent stability and control characteristics.

The mission performance method provided numerous quantities of interest that were each interpolated with radial basis functions to generate individual surrogate models. These include: max takeoff gross weight (MTOW); lift-coefficient and lift-to-drag ratio at initial, mid, and final cruise points; optimum cruise altitude; block fuel and total fuel; takeoff field length; second segment climb gradient; landing weight and landing field length; approach velocity and touchdown velocity. Figure 12 illustrates RBF model contours for four outputs, as well as the training samples and validation samples. The validation cases demonstrated excellent agreement between the RBF model and the mission

performance method, as shown in Figure 13. Of note is the “infeasible planform zone” in the model contour plots, which designates combinations of total planform area with OEW as being infeasible with respect to a constraint specified within the mission performance method. These planforms typically failed to make takeoff field length limits and climb gradient limits. The RBF model of takeoff field length also interpolated through poorly converged combinations of planform and OEW near the 15000 foot contour level, thereby leading to spurious values of field length that made the model less smooth near that boundary.

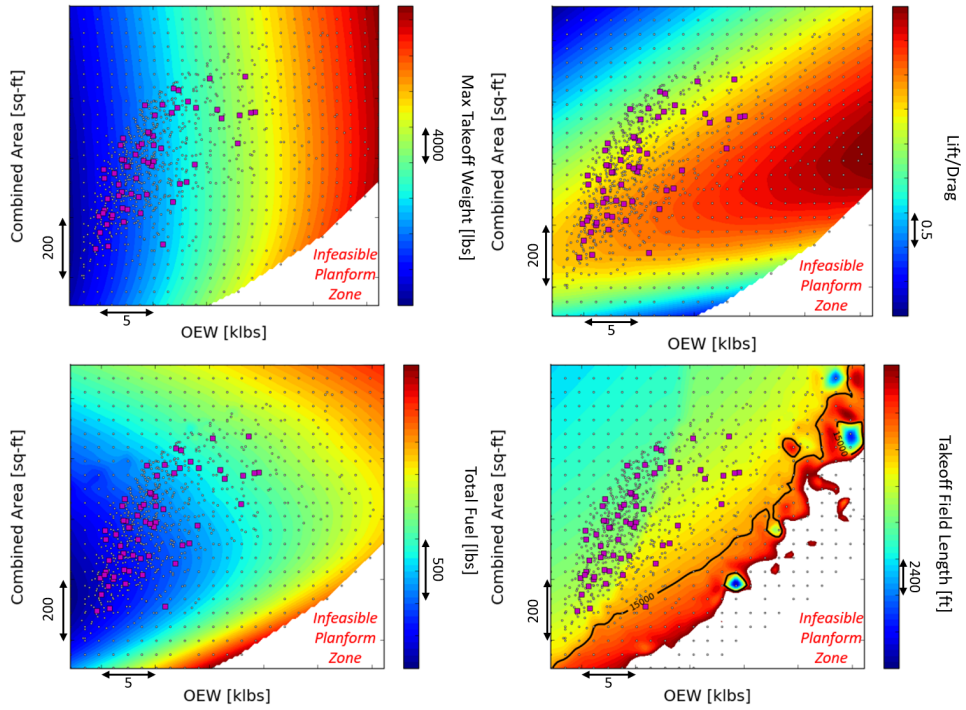

Figure 12 – Four example RBF surrogate models with training samples (circles) and validation samples (squares) representing outputs from the mission performance method.

3.6 Structural Performance Method

A higher-fidelity procedure for assessing structural integrity and mass properties was included in the framework after this study was completed. Instead of relying on the RBF surrogate models for mass properties estimates, where the RBF training dataset was derived with assumed loads and structural layout in the mass properties method, a finite element beam model for Nastran solution 144 was developed for automatic execution. This method provided shear, moment, and torsion results that sized an assumed wing box layout instead, followed by a structural weight estimate for the existing mass properties method. An iterative loop, as shown in Figure 14, enabled converging a planform jig shape in order for the structural beam model to be deflected properly under the 1g aerodynamic loads obtained from the aerodynamic shape optimization method. In this manner the mass properties were consistent with the structural response and the computed wing box sizing for the load cases considered. The outcome of the procedure was greater fidelity in the estimate of OEW and center of gravity location for a mission performance assessment.

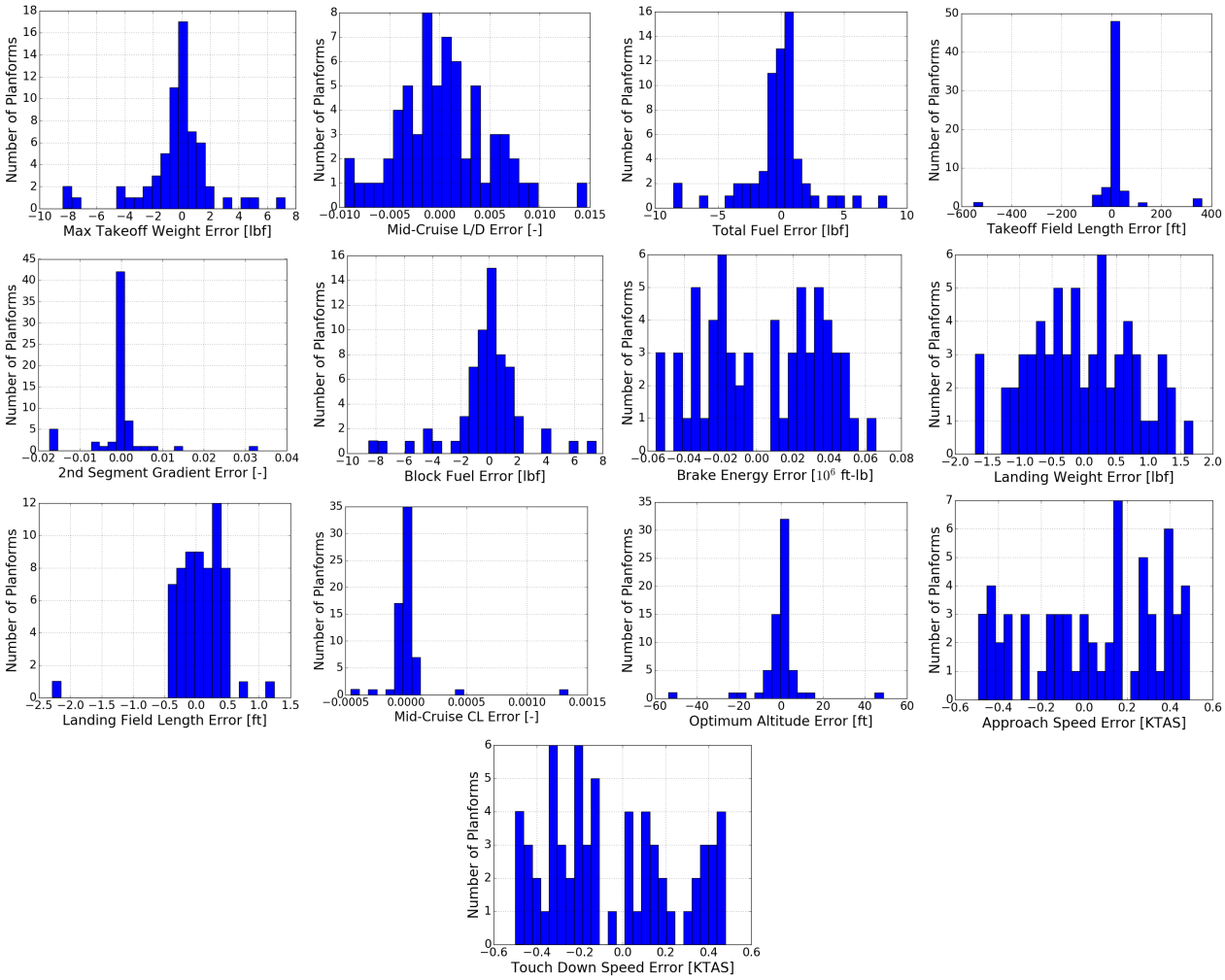

Figure 13 – Histograms of the output error between the RBF model and mission performance method predictions from the validation cases.

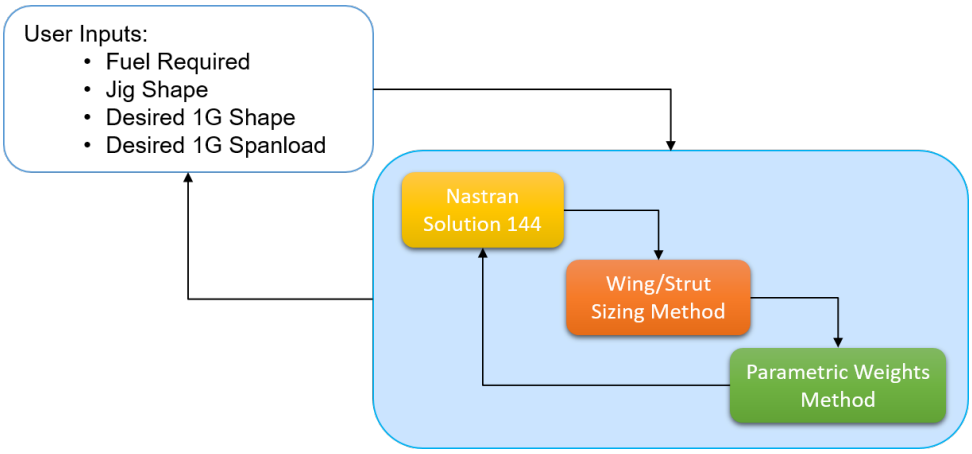

Figure 14 – A convergence loop between an external loads, internal wing box sizing, and parametric weights method provided consistency between aerodynamic loads and structural deflections.

4 Planform Design Exploration Case Study

The geometry and analysis processes described in Sections 2 and 3 were launched by a design exploration manager named MDOPT. As shown in Figure 15, this system managed user inputs to conduct multiple design exploration activities. Individual or batch instances of new planforms could be processed, either manually defined or using an orthogonal array sampling approach for a design of experiments (DOE) exercise. Subsequently Kriging surrogate models could be built using design variables as inputs and any analysis outputs as responses. Various optimizer options were also available to conduct a design search based on the surrogate models, which included model updates as the optimizer tested candidate designs. Data flow, post-processing, and job management on a computing cluster were all managed within the MDOPT environment.

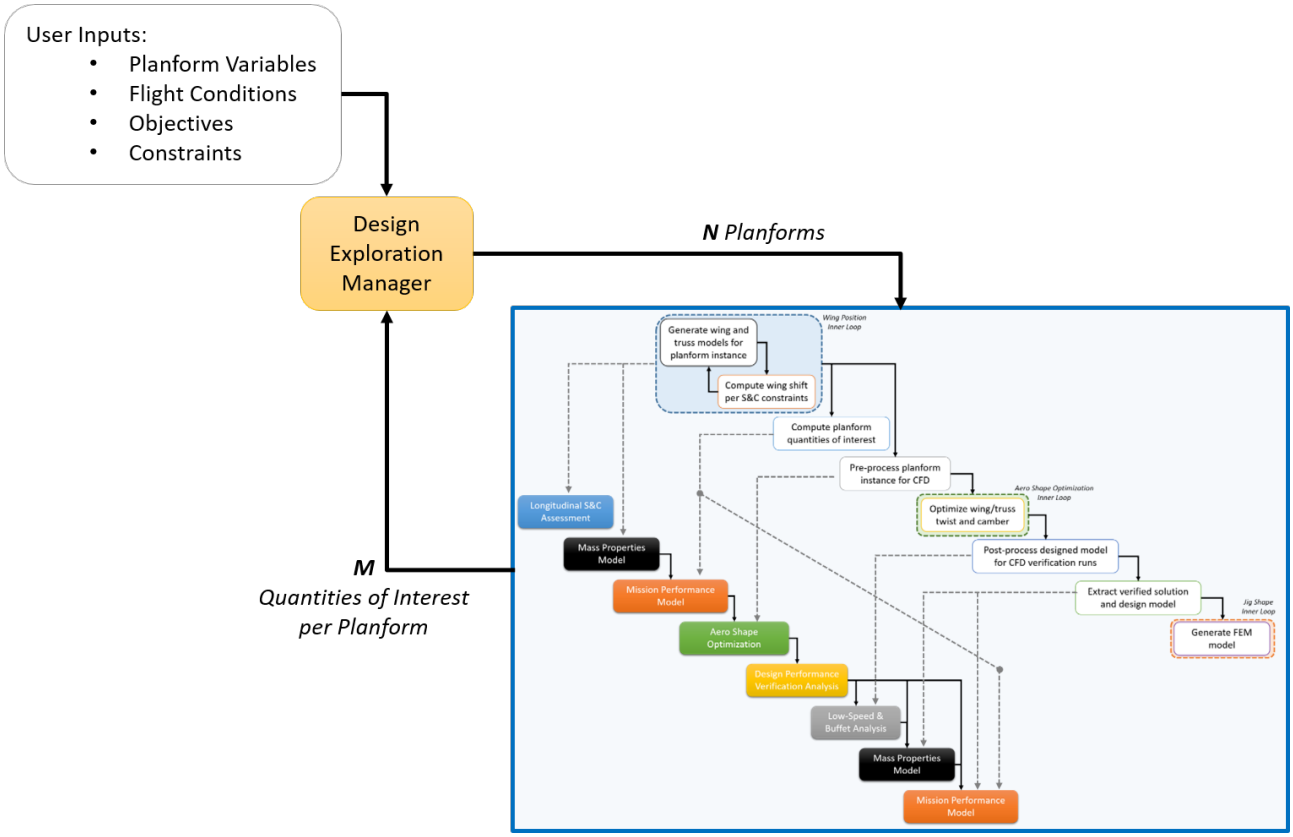

Figure 15 – The MDOPT design exploration manager executed the full analysis suite for any candidate planform stemming from a DOE, optimizer search, or user-defined instance.

In this effort a DOE was initialized with 64 planform instances based on the number of design variables in the planform parameterization and the available time to complete the study. Example planforms are shown in Figure 16 that represent a variety of wing span, wing area, truss attachment locations, sweep, and chord distributions made possible by the parameterization. The full analysis sequence was executed for all planforms with at most 25 planforms running simultaneously on the computing cluster, taking approximately 1.5 weeks to complete due to the Tranair aerodynamic shape optimization inner-loop. Two-dimensional slices of the design space are shown in Figure 17, where each colored symbol represents the performance of a different planform according to the given color-bar. An interpolation of the DOE results is also shown to illustrate the model evolution during optimization as it adapts to new candidate planforms. In this first slice of the objective space two regions appear promising for aerodynamic performance.

A drag minimization problem was defined after interpolating Kriging models through the DOE results. Other mission performance metrics were available to define the objective function, yet the Tranair drag estimate was selected for minimization since the updates to the seed aerodynamic database in the mission performance method had not yet been implemented as a function of planform–only modifications to a drag buildup were provided as a function of planform. Constraints were active within

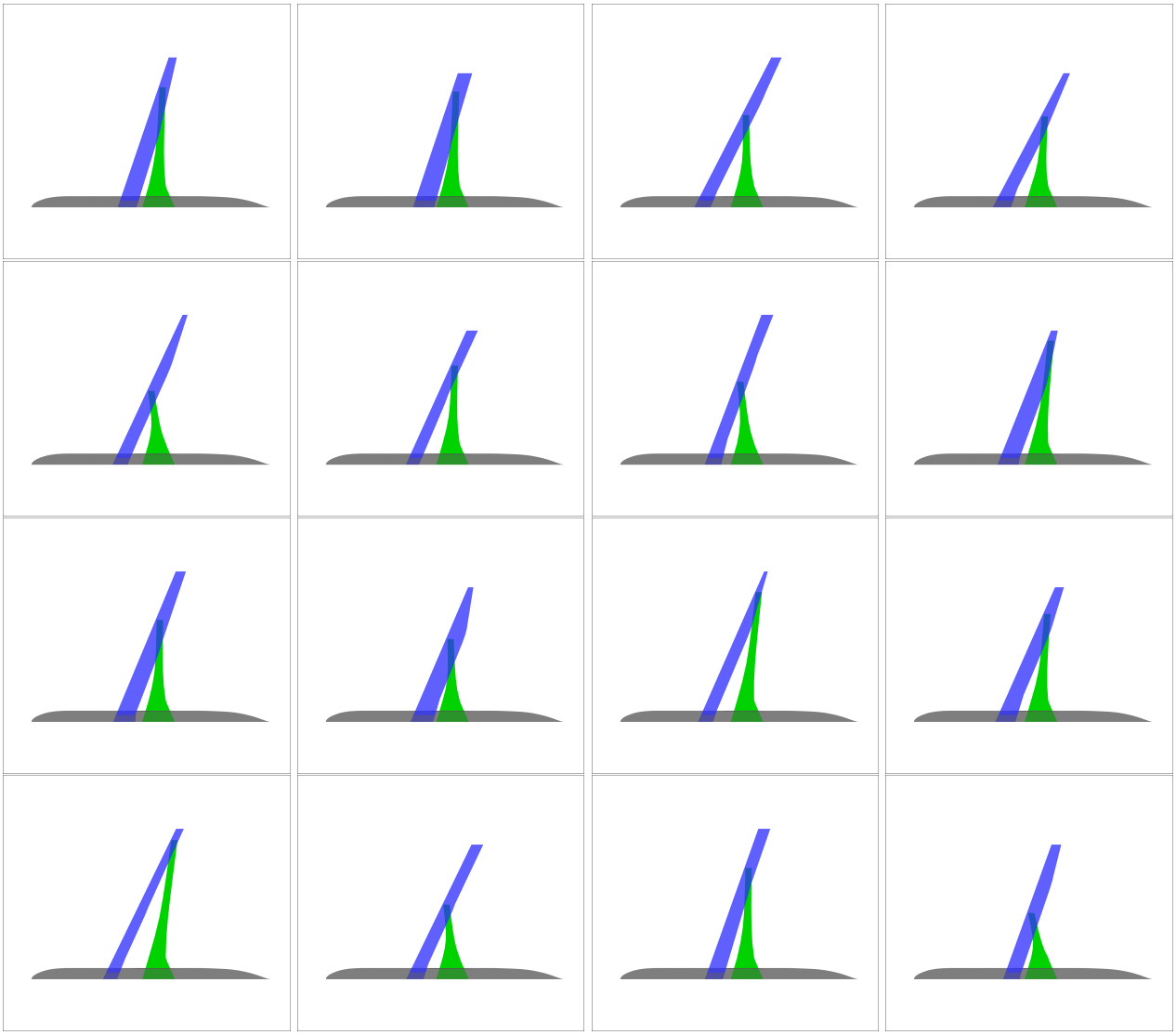

Figure 16 – Example planforms generated in a DOE exercise via an orthogonal array sampling of the design space.

each inner-loop process of the MDAO framework, such as in the definition of the aerodynamic shape optimization problem, however in the top-level planform optimization no constraints were explicitly defined beyond setting side bounds to the design variables.

The planform optimization problem was allowed to progress over seven design iterations during the allotted study period. Figures 18 through 20 are a sequence of plots that show the introduction of candidate planforms during the optimization search, along with updates to the performance model that depict the emergence of promising regions in the design space. This optimization procedure found a candidate design with an improved performance of $\Delta(L/D) = +0.5$ over the seed model. Compared to the seed in Figure 21, this candidate planform had higher wing aspect ratio, higher wing sweep, and higher wing area. The truss also attached further inboard on the wing.

Note that the performance shown in Figures 17 through 20 is a function of the eight design variables applied together, thus visual trends based on the two design variables alone may not provided sufficient insight about TTBW planform design. For example, in these design space slices a low L/D result may not be the consequence of a poor combination of wing aspect ratio and total planform area, but rather the choice of values for one or more of the other six design variables (e.g., wing sweep).

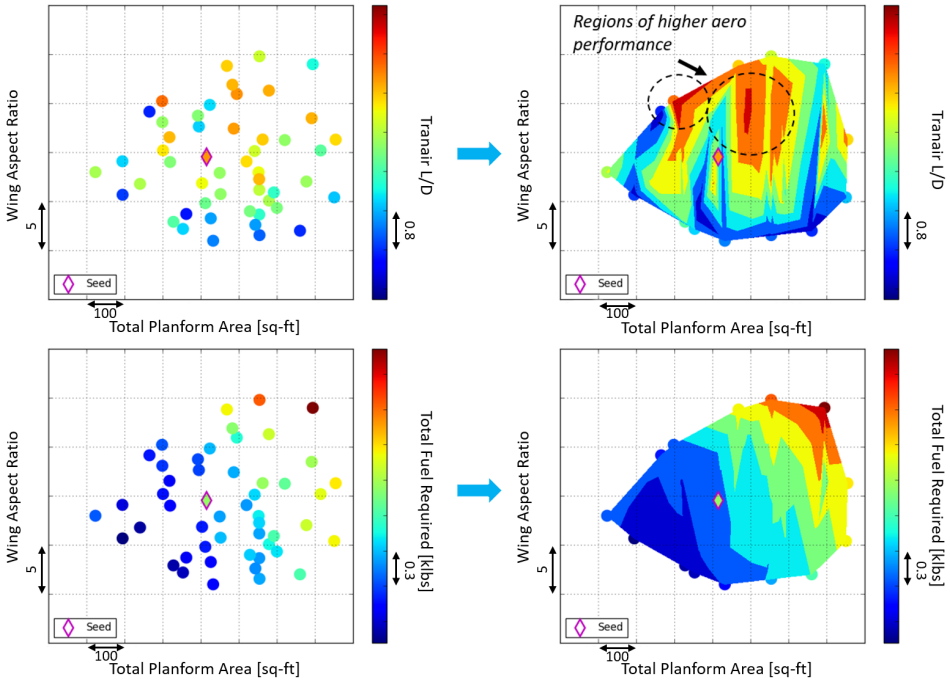

Figure 17 – DOE results for 64 planform instances are shown with respect to wing aspect ratio and total planform area, including a surrogate model representation interpolated through the data.

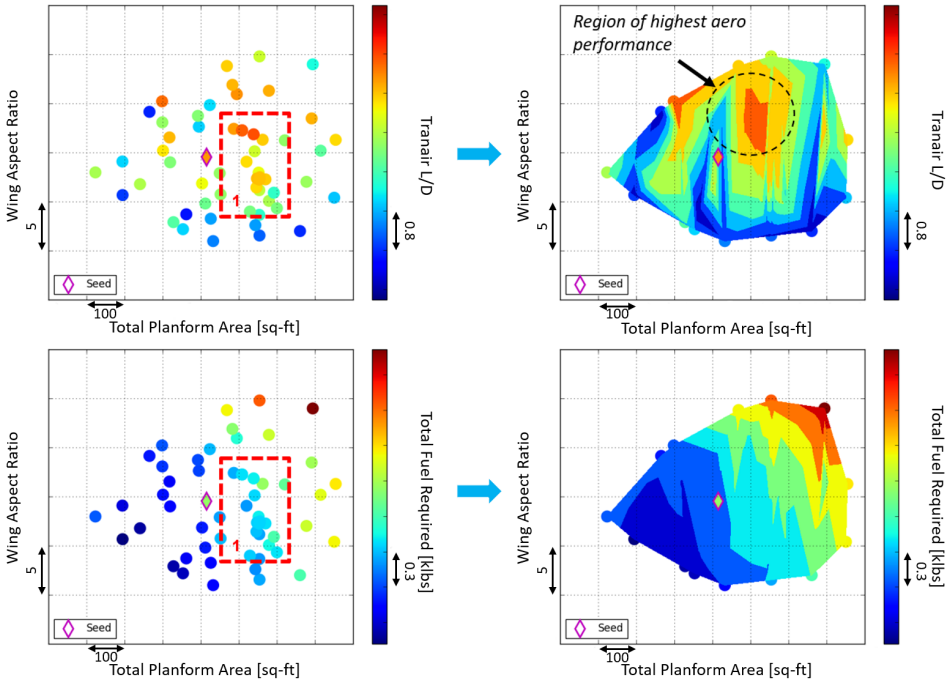

Figure 18 – Candidate designs added in the first design iteration by the optimizer.

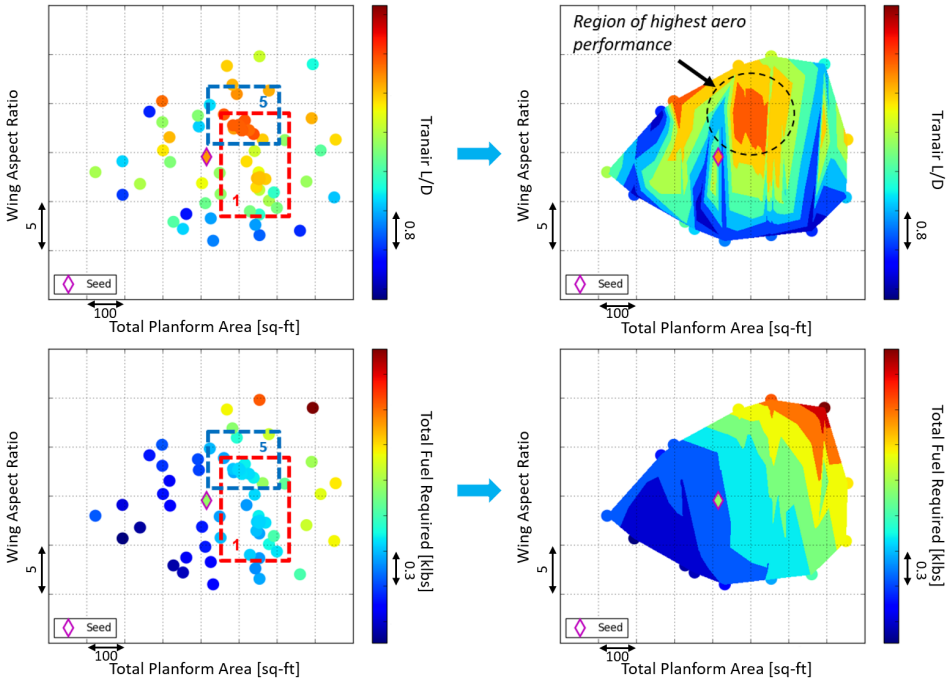

Figure 19 – Candidate designs added in the fifth design iteration by the optimizer.

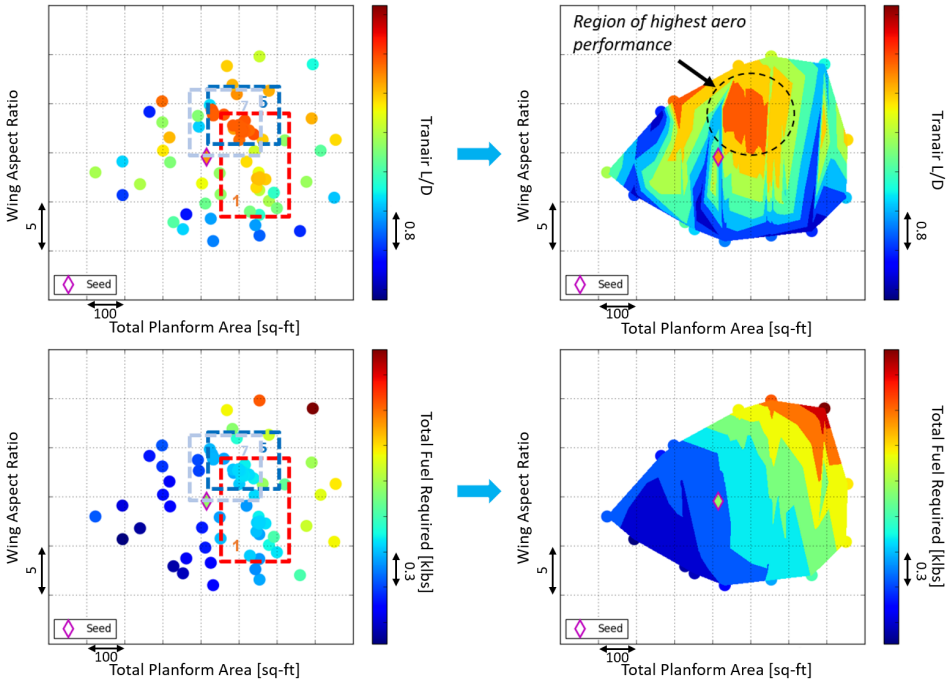

Figure 20 – Candidate designs added in the seventh (and final) design iteration by the optimizer.

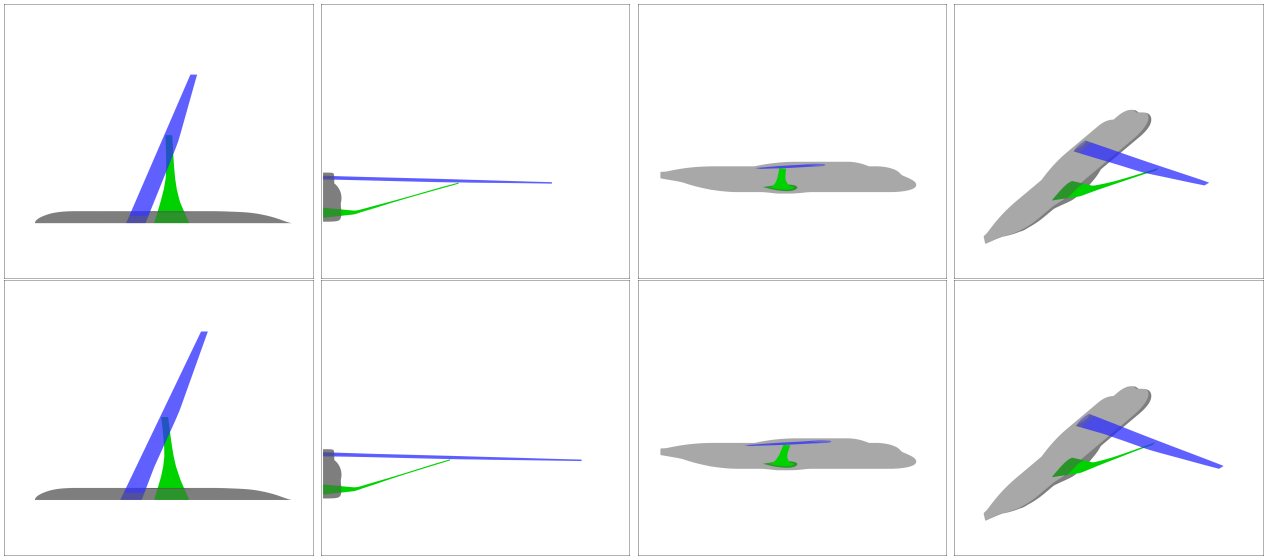

Figure 21 – The top row portrays the seed model and the bottom row depicts the planform with the highest $\Delta(L/D) = +0.5$ found by the optimizer in this study.

5 Summary

This effort presented the development of a MDAO framework specifically designed for planform design exploration of TTBW configurations. Each analysis method exhibited higher fidelity than is typically represented in MDAO frameworks, such as in multi-point aerodynamic shape optimization, stability and control, mass properties, and mission performance. Each method was directly implemented into the framework or represented through the use of RBF surrogate models, which enabled bypassing the large cost and complexity of directly connecting a mass properties method and mission performance method. Despite the additional computational expense incurred by these methods, the framework satisfied the requirement of searching for improved planforms while generating 3D models of sufficient maturity for subsequent fine-tuning of its designed surfaces. A drag minimization case study was presented that demonstrated a successful design exploration of TTBW planforms, where an optimizer search resulted in candidate planforms with improved performance compared to a previously designed seed model.

6 Acknowledgments

Many subject matter experts provided both consulting and methods development for the MDAO framework presented in this work. The following are acknowledged for their contributions: Leo Chou (mission performance), Paul Dees (configuration), Eric Dickey (aerodynamics), Jeff Jonokuchi (stability and control), Tobin Lee (mass properties), Brandin Northrop (mass properties), Khanh Pham (mission performance), Eric Reichenbach (structures), Dino Roman (aerodynamics), Will Sampedro-Thompson (structures), Tony Sclafani (aerodynamics), Alan Simonini (configuration), and John Vassberg (aerodynamics).

7 Contact Author Email Address

The author may be contacted at this email address: david.s.lazzara@boeing.com

8 Copyright Statement

References

[1] Bradley, M., Droney, C. 'Subsonic Ultra Green Aircraft Research: Phase I Final Report', NASA CR-2011-216847, 2011.

[2] Bradley, M., Droney, C. 'Subsonic Ultra Green Aircraft Research: Phase II: N+4 Advanced Concept Development ', NASA CR-2012-217556, 2012.

[3] Bradley, M., Droney, C. 'Subsonic Ultra Green Aircraft Research: Phase II Final Report', NASA CR-2015-218704/VOL2, 2015.

[4] Bradley, M., Allen, T., Droney, C. 'Subsonic Ultra Green Aircraft Research: Phase II–Volume III–Truss Braced Wing Aeroelastic Test Report', NASA CR-2015-218704, 2014.

[5] Delavenne, M. et al. 'Multidisciplinary analysis and design of strut-braced wing concept for medium range aircraft', AIAA SCITECH 2022 Forum. doi: 10.2514/6.2022-0726, 2022.

[6] Droney, C., Sclafani, T., Harrison, N., Grasch, A., Beyar, M. 'Subsonic Ultra Green Aircraft Research: Phase III–Mach 0.75 Transonic Truss-Braced Wing Design', NASA CR-20205005698, 2020.

[7] Xiong, J., Nguyen, N., Bartels, R. 'Aerodynamic Optimization of Mach 0.8 Transonic Truss-Braced Wing Aircraft Using Variable Camber Continuous Trailing Edge Flap', AIAA SCITECH 2022 Forum. doi: 10.2514/6.2022-0016, 2022.

[8] Xiong, J., Nguyen, N., Bartels, R. 'Aeroelastic Trim Drag Optimization of Mach 0.8 Transonic Truss-Braced Wing Aircraft with Variable Camber Continuous Trailing Edge Flap', AIAA AVIATION 2022 Forum. doi: 10.2514/6.2022-4150, 2022.

[9] Nguyen, N., Xiong, J., Fugate, J. 'Multi-point Jig Twist Optimization of Mach 0.745 Transonic Truss-Braced Wing Aircraft and High-Fidelity CFD Validation', AIAA Scitech 2021 Forum. doi: 10.2514/6.2021-0338, 2021.

[10] Harrison, N., Gatlin, G., et al. 'Development of an Efficient Mach=0.80 Transonic Truss-Braced Wing Aircraft', AIAA SciTech Forum, Orlando, Florida, United States, AIAA-2020-0011, January 2020.

[11] Harrison, N., Gatlin, G., et al. 'Transonic Truss-Braced Wing Vision Vehicle Technology Maturation'. 33rd Congress of the International Council of Aeronautical Sciences, Stockholm, Sweden, ICAS-2022-0397, September 2022.

[12] Hwang, J., Kenway, G., Martins, J. 'Geometry and Structural Modeling for High-Fidelity Aircraft Conceptual Design Optimization', 15th AIAA/ISSMO Multidisciplinary Analysis and Optimization Conference. doi: 10.2514/6.2014-2041, 2014.

[13] Ivaldi, D. et al. 'Aerodynamic Shape Optimization of a Truss-Braced-Wing Aircraft', 16th AIAA/ISSMO Multidisciplinary Analysis and Optimization Conference. doi: 10.2514/6.2015-3436, 2015.

[14] Variyar, A., Economon, T., Alonso, J. 'Design and Optimization of Unconventional Aircraft Configurations with Aeroelastic Constraints', 55th AIAA Aerospace Sciences Meeting. doi: 10.2514/6.2017-0463, 2017.

[15] Johnson, F. et. al. 'TranAir: A full-potential, solution-adaptive, rectangular grid code for predicting subsonic, transonic, and supersonic flows about arbitrary configurations.' User manual. NASA CR-4349, 1992.

[16] Sarojini, D. et al. 'Parametric Wingbox Structural Weight Estimation of the CRM, PEGASUS and Truss-Braced Wing Concepts', AIAA AVIATION 2022 Forum. doi: 10.2514/6.2022-4054, 2022.

[17] Xiong, J., Bartels, R., Nguyen, N. 'Aerodynamic Optimization of Mach 0.745 Transonic Truss-BracedWing Aircraft with Variable-Camber Continuous Trailing-Edge Flap', AIAA Scitech 2021 Forum. doi: 10.2514/6.2021-0337, 2021.

[18] Xiong, J., Bartels, R., Nguyen, N. 'Aeroelastic Trim Drag Optimization of Mach 0.745 Transonic Truss-BracedWing Aircraft with Variable-Camber Continuous Trailing-Edge Flap', AIAA AVIATION 2021 FORUM. doi: 10.2514/6.2021-2528.

[19] Ting, E. et al. 'Aerodynamic Analysis of the Truss-Braced Wing Aircraft Using Vortex-Lattice Superposition Approach', 32nd AIAA Applied Aerodynamics Conference. doi: 10.2514/6.2014-2597, 2014.

[20] Variyar, A., Economon, T., Alonso, J. 'Multifidelity Conceptual Design and Optimization of Strut-Braced Wing Aircraft using Physics Based Methods', 54th AIAA Aerospace Sciences Meeting. doi: 10.2514/6.2016-2000, 2016.

[21] Xiong, J., Nguyen, N., Fugate, J. 'Jig Twist Optimization of Mach 0.745 Transonic Truss Braced Wing Aircraft and High-Fidelity CFD Validation', AIAA Scitech 2020 Forum. doi: 10.2514/6.2020-0451, 2020.